Scientific Research Publishing

World Journal of Nano Science and Engineering, 2026, 16(3), 98-117
https://www.scirp.org/journal/wjnse
ISSN Online: 2161-4962
ISSN Print: 2161-4954

Effect of NaCl Highly Textured Crystalline Substrates on the Raman Response of Graphene

Rafael Antolin-Jimenez, Doroteo Mendoza López

Instituto de Investigaciones en Materiales, Universidad Nacional Autónoma de México, CDMX, México
Email: rafaelantolinjimenez@ciencias.unam.mx, doroteo@unam.mx

How to cite this paper: Antolin-Jimenez, R. and López, D.M. (2026) Effect of NaCl Highly Textured Crystalline Substrates on the Raman Response of Graphene. *World Journal of Nano Science and Engineering*, **16**, 98-117.
https://doi.org/10.4236/wjnse.2026.163005

Received: June 7, 2026
Accepted: September 4, 2026
Published: September 7, 2026

Abstract

The interaction between graphene and the substrate on which it is supported plays a fundamental role in determining its optical and electronic properties. In this work, multilayer graphene samples were synthesized through mechanical exfoliation and deposited onto conventional Si/SiO_2 substrates and NaCl highly textured crystalline substrates. Optical contrast microscopy and Raman spectroscopy were employed to determine the number of graphene layers and to evaluate substrate-induced effects. Unlike graphene on Si/SiO_2, graphene deposited on NaCl exhibited negative optical contrast and reduced wavelength dependence. Raman analysis revealed substrate dependent doping behavior: graphene on SiO_2 presented predominant p-type doping, whereas graphene on NaCl showed a tendency toward n-type doping with strain contributions dominating the spectral shifts. Carrier concentrations were estimated to be on the order of 10^{12} cm^{-2}. These results demonstrate the strong influence of ionic crystalline substrates on graphene properties and highlight NaCl as a promising platform for studying electrostatic substrate effects in two-dimensional materials.

Keywords

Graphene, Multilayer Graphene, NaCl, Raman Spectroscopy, Optical Contrast, Two-Dimensional Materials, Substrate Effects

1. Introduction

Since its experimental isolation by Andre Geim and Konstantin Novoselov in 2004, graphene has attracted enormous scientific interest due to its exceptional electronic, mechanical, and optical properties [1]. Graphene consists of a single atomic layer of carbon atoms arranged in a two-dimensional hexagonal honeycomb lattice, behaving as a semimetal with massless Dirac fermions and extraor-

dinarily high carrier mobility. It is characterized by a zero band gap, with the valence and conduction bands meeting at the Dirac point. This unique electronic structure gives rise to a pronounced ambipolar electric field effect, in which both electrons and holes can be induced as majority charge carriers through the application of external electric fields. Carrier concentrations on the order of 10^{13} cm^{-2} and room-temperature mobilities approaching 10^4 cm^2/Vs have been reported, surpassing those of many conventional semiconductors [1].

In addition to its remarkable electronic properties, graphene also exhibits extraordinary mechanical behavior. Nanoindentation measurements performed by atomic force microscopy on suspended monolayer graphene membranes have demonstrated its exceptional elastic response and intrinsic strength. By fitting the stress-strain behavior, second- and third-order elastic stiffness constants of approximately 340 N/m and 640 N/m, respectively, have been obtained, together with an intrinsic strength close to 42 N/m. These values correspond to an effective Young's modulus of approximately 1TPa, establishing graphene as one of the strongest materials ever measured [2] [3].

Graphene and few-layer graphene systems have therefore been extensively investigated due to their outstanding electronic, mechanical, and optical properties, making them highly promising materials for applications in microelectronics, optoelectronics, and sensing devices. However, in most practical and experimental applications, graphene does not exist as an isolated system but rather supported on a solid substrate, which is essential for its manipulation, characterization, and eventual integration into devices.

Conventional studies commonly employ Si/SiO_2 substrates for graphene characterization, because they provide suitable optical contrast for graphene identification. Nevertheless, numerous studies have demonstrated that the electronic and vibrational properties of graphene strongly depend on its surrounding environment, particularly on the supporting substrate [4]-[8]. In particular, substrates may induce unintended doping, modify carrier mobility, and produce shifts in the characteristic Raman bands, effects that cannot be explained solely by weak van der Waals interactions. Recent investigations suggest that surface charges, structural defects, and substrate related electrostatic phenomena play a crucial role in the graphene-substrate interaction, directly influencing the electrical and optical behavior of the material [4]. Consequently, alternative insulating and crystalline substrates have gained attention to better understand interfacial phenomena. For instance, crystalline oxide substrates like sapphire can alter both doping and strain due to strong interfacial coupling [9], whereas highly charged ionic surfaces such as mica induce pronounced electrostatic gating effects [10].

In this context, highly textured ionic crystalline substrates like NaCl are especially attractive due to their periodic electrostatic potential and dielectric nature. Their ionic character makes them suitable platforms to investigate how specific surface configurations and ionic lattices modulate the electrostatic and mechanical properties of graphene [11]. The alternating arrangement of Na^+ and Cl^- ions

(see Figure 1) may influence graphene through electrostatic interactions. Despite this potential, studies involving mechanically exfoliated graphene deposited on NaCl substrates remain scarce.

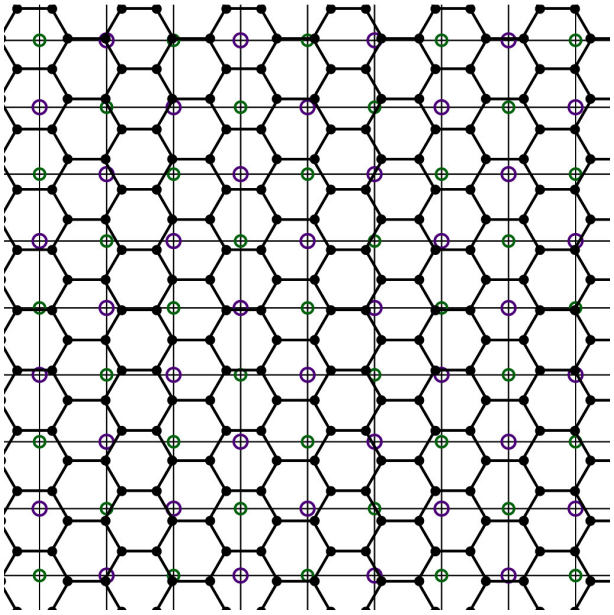

Figure 1. Scaled schematic representation of a graphene monolayer placed on the surface of a NaCl single crystal. Green and purple spheres denote sodium (Na) and chlorine (Cl) atoms, respectively. The carbon-carbon bond length in graphene is 1.42 Å, whereas the Na-Cl nearest-neighbor distance is 2.82 Å.

The main objective of this work is to investigate the influence of NaCl substrates on the optical and electronic properties of graphene using optical contrast microscopy and Raman spectroscopy as non-destructive optical characterization techniques.

2. Experimental Methods

2.1. Graphene Synthesis

Graphene and multilayer graphene samples were obtained by mechanical exfoliation of graphite kish grade 50 using adhesive scotch tape [12]. Independent exfoliation procedures were carried out on Si/SiO_2 substrates (University Wafer, 306 nm oxide thickness) and on NaCl substrates (Z123595, Sigma-Aldrich). The graphene flakes analyzed on NaCl were not transferred from the Si/SiO_2 substrates; instead, separate graphene flakes were produced directly on each substrate. After exfoliation, suitable flakes were identified by optical contrast microscopy and subsequently characterized by Raman spectroscopy.

Prior to graphene deposition, the NaCl substrates were used as received from the supplier and cleaned with acetone. Sample handling was performed using gloves to minimize contamination. Graphene deposition and subsequent optical and Raman characterization were carried out under ambient laboratory condi-

tions. Between characterization sessions, the samples were stored in a vacuum chamber to reduce exposure to atmospheric moisture. Nevertheless, due to the hygroscopic nature of NaCl, the presence of adsorbed water at the surface cannot be completely excluded and may contribute to the variability of the observed doping and strain effects.

2.2. Characterization Techniques

Several characterization methods were employed:

2.2.1. X-Ray Diffraction (XRD)

XRD measurements (Bruker AXS model D8 Advance) were carried out in a $\theta - 2\theta$ configuration using $CuK\alpha$ radiation ($\lambda = 1.54050$ Å) in order to verify the crystalline structure and orientation of the NaCl substrates by comparing the obtained diffraction patterns with the standard NaCl data reported by the National Institute of Standards and Technology (NIST).

2.2.2. UV-Vis Spectroscopy

UV-Vis spectroscopy was used to evaluate the optical transparency of NaCl substrates in the visible spectral region (see the inset of **Figure 3(b)**). Transmittance and reflectance measurements were carried out in the ultraviolet-visible range using a Shimadzu UV-2600 spectrophotometer. These measurements allowed the direct determination of the optical response of NaCl within the spectral range of interest, and the obtained data were subsequently used for the experimental calculation of the refractive index.

2.2.3. Atomic Force Microscopy

The surface topography and roughness parameters of the NaCl substrates were characterized by Atomic Force Microscopy (AFM, JSPM-4210) operated in tapping mode under ambient conditions. AFM images were acquired over a scan area of $2 \times 2, \mu m^2$, and the root-mean-square (RMS) roughness (R_q) was extracted from the measured height distribution.

2.2.4. Optical Contrast Microscopy

The determination of the number of layers in the multilayer graphene samples was carried out using two complementary techniques: optical contrast microscopy and Raman spectroscopy. Once synthesized, the samples were initially analyzed by optical contrast microscopy using an IRONSCOPE optical microscope equipped with a 100× objective lens (Nikon 332384) in order to identify graphene flakes and estimate the number of layers. The samples were illuminated under normal incidence using a Tungsten white light source, and images of the exfoliated graphene were acquired with a Celestron 5MP Digital Microscope Imager digital camera.

Following the identification of the graphene flakes and substrate areas using the ImageJ software [13], the acquired white-light images were decomposed into their red (R), green (G), and blue (B) components. Intensity values ranging from 0 to

255 were then extracted from the corresponding color histograms. The optical contrast of each graphene flake was determined experimentally by comparing the intensity measured over the graphene-covered region with that of the uncovered substrate, as defined in Equation (1).

The optical contrast was defined as:

$$C = \frac{I_s - I_g}{I_s} \text{SEQ Ecuacion 1} \tag{1}$$

where I_s and I_g correspond to the reflectance of the substrate and graphene-covered regions, respectively.

Prior to the experimental analysis, theoretical calculations of the optical contrast of graphene on the different substrates employed in this work were carried out. These calculations made it possible to optimize the processing of the experimental images and to select the most suitable color channel for optical contrast quantification, thereby improving the estimation of the number of graphene layers.

For the theoretical calculation of the optical contrast as a function of wavelength, the Transfer Matrix Method (TMM) was employed, since it provides a compact formalism for incorporating the effects of multiple thin films. The transfer matrix of a thin film is given by Equation (2) [14].

$$M_i = \begin{bmatrix} \cos k_i l_i & \frac{i}{n_i}\sin k_i l_i \\ i n_i \sin k_i l_i & \cos k_i l_i \end{bmatrix} \tag{2}$$

where n_i is the refractive index of the film $k_i = \frac{2\pi n_i}{\lambda_0}$ and l_i is the thickness of the film.

The transfer matrix of the complete multilayer system is then obtained simply as the matrix product of the individual transfer matrices corresponding to each film.

$$M = M_1 M_2 M_3 \cdots M_N = \begin{bmatrix} A & B \\ C & D \end{bmatrix} \tag{3}$$

From this, it follows that the reflection coefficient of the multilayer system is ultimately given by Equation (4).

$$r = \frac{An_0 + Bn_T n_0 - C - Dn_T}{An_0 + Bn_T n_0 + C + Dn_T} \tag{4}$$

where n_0 is the refractive index of the medium preceding the multilayer system, which in our case corresponds to air, and n_T is the refractive index of the medium following the multilayer system, corresponding in our case to Si or NaCl for the Si/SiO_2 and NaCl substrates, respectively. In the theoretical treatment, both media are assumed to be semi-infinite [15].

Finally, by applying Equation (4) to our particular case, the optical contrast of graphene on each of the employed substrates (see **Figure 2**) is evaluated using

Equation (1) together with the reflected irradiance $I = |r|^2$. This approach allows the dependence of the optical contrast on the wavelength of the incident radiation to be analyzed.

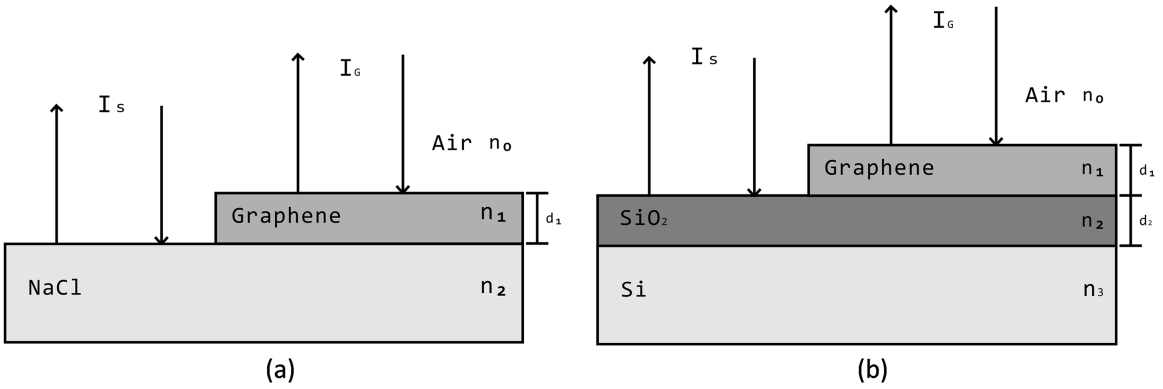

Figure 2. Schematic representations of the graphene-substrate system under illumination, used for the measurement of its optical contrast. (a) Illustrative diagram of the NaCl—graphene substrate system. (b) Illustrative diagram of the Si/SiO_2—graphene system.

2.2.5. Raman Spectroscopy

The same regions previously analyzed by optical microscopy were subsequently characterized by Raman spectroscopy in order to evaluate the structural quality, determine the number of graphene layers, and analyze doping and strain effects. The measurements were carried out using an EnSpectr R532 spectrometer equipped with a 532 nm excitation laser and providing a spectral resolution of 4 - 6 cm^{-1}. For spectral acquisition, a 40× objective lens was employed, together with a laser power corresponding to 40% of the maximum output power and an average of 1000 samplings per measurement. Particular attention was given to the G and 2D Raman bands.

The G band (approximately 1580 cm^{-1}) is associated with in-plane optical phonons, while the 2D band (approximately 2700 cm^{-1}) provides information regarding the number of graphene layers [16]-[18].

A total of 21 graphene flakes on Si/SiO_2 and 35 graphene flakes on NaCl, with thicknesses ranging from one to five layers, were analyzed by optical microscopy. The Si/SiO_2 flakes were distributed among 13 independent substrate chips, whereas the NaCl flakes were collected from five different regions of the same substrate. Raman characterization was subsequently performed on the same flakes, acquiring two spectra per flake, resulting in 42 spectra for Si/SiO_2 and 70 spectra for NaCl.

For the monolayer graphene samples used in the $\omega_G - \omega_{2D}$ correlation analysis, the G and 2D bands were fitted with single Lorentzian functions. Peak positions were extracted from the fitted center-frequency parameters. The uncertainty associated with each peak position was obtained by combining in quadrature the fitting uncertainty returned by the fitting routine and the instrumental uncertainty associated with the Raman spectrometer resolution (±2 cm^{-1}).

It is worth noting that although the spectral resolution of the Raman spectrometer is approximately 4 - 6 cm^{-1}, the uncertainty in determining the peak positions (ω_G and ω_{2D}) is considerably smaller. Peak centers were obtained through Lorentzian fitting of spectra with high signal-to-noise ratios, resulting in fitting uncertainties typically below ±0.2 cm^{-1}. Moreover, the instrumental response function primarily contributes to symmetric peak broadening, affecting the measured full width at half maximum (FWHM) rather than systematically shifting the peak center positions. Consequently, the determination of relative Raman shifts ($\Delta\omega$) remains sufficiently accurate for the strain and doping analysis presented here. To provide a conservative estimate of the uncertainty, the instrumental resolution was included in the error analysis together with the fitting uncertainty.

The uncertainties of the reference frequencies of charge-neutral graphene were taken from the same literature source used for the reference values [19]. Uncertainties in the strain-doping decomposition, Fermi energy, and carrier concentration were calculated using standard uncertainty propagation based on the root-sum-square of the corresponding partial derivatives and the uncertainties of the independent variables.

3. Results and Discussion

In this section, we systematically evaluate how highly textured ionic NaCl substrates influence the optical contrast and electronic properties of graphene in comparison with conventional Si/SiO_2 substrates. The discussion is organized into four stages. First, the structural and optical properties of the NaCl substrates are characterized by X-ray diffraction (XRD) and UV-Vis spectroscopy to verify their crystallinity and optical transparency. Second, mechanically exfoliated graphene flakes are transferred onto both substrate architectures. Third, optical contrast microscopy is employed as a rapid, nondestructive method to locate graphene flakes and assess their thickness through comparison with theoretical reflectance calculations. Finally, Raman spectroscopy is used to confirm the graphene layer number and to quantitatively separate the effects of mechanical strain and charge doping through vector decomposition of the G and 2D Raman band shifts. Together, these analyses provide insight into how the structural and optical characteristics of the substrate influence the optical visibility and electronic response of graphene.

3.1. Characterization of NaCl Substrate

The diffraction patterns exhibited sharp reflections characteristic of the face-centered cubic (FCC) structure (**Figure 3(a)**), with a pronounced preferential orientation along the (200) direction, indicating a high degree of crystallinity.

UV-Vis spectroscopy measurements confirmed the high transparency of the NaCl substrate throughout the visible spectral range. This characteristic can be qualitatively appreciated in the insect of **Figure 3(b)** where a photograph of the crystal is presented.

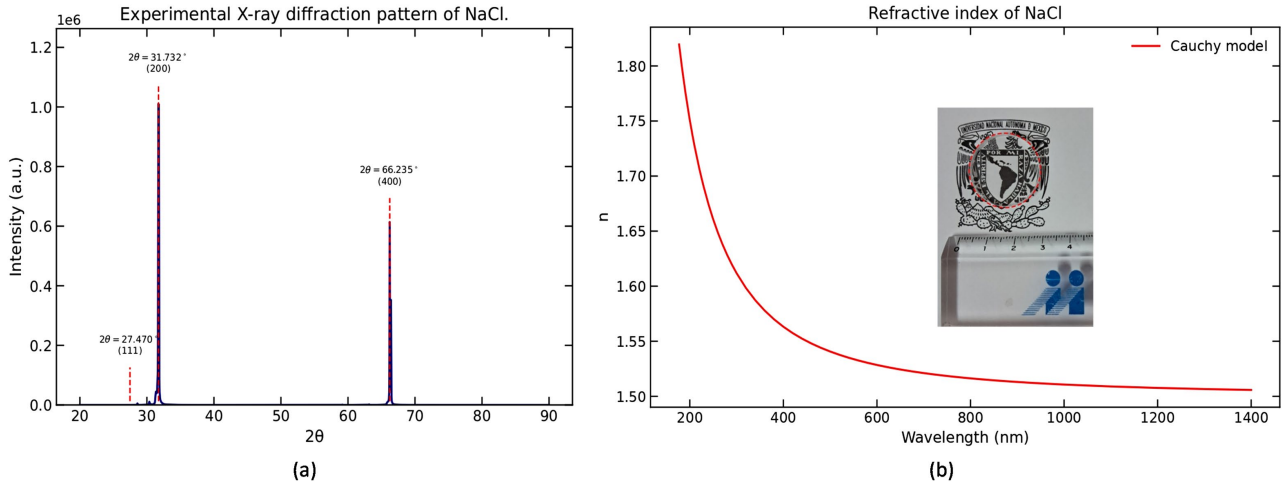

Figure 3. (a) X-ray diffraction pattern of the NaCl substrate, showing the predominance of the (200) reflection together with the presence of its harmonic (400), characteristic peaks associated with the halite-type crystal structure. (b) Refractive index of the NaCl substrate fitted using the second-order Cauchy model. The inset shows a photograph of the NaCl substrate (Z123595, Sigma-Aldrich) used in this work, with the sample edge highlighted in red.

The refractive index of the NaCl substrate was determined by fitting the experimental transmittance spectrum with a Fabry-Pérot interference model. Since the NaCl crystal has a finite thickness d = 4 mm multiple internal reflections occur within the sample, producing interference effects that modulate the transmitted intensity. These effects were explicitly included in the theoretical transmittance model.

To describe the wavelength dependence of the refractive index, a second-order Cauchy dispersion relation was assumed, where A_n and B_n are fitting parameters. In addition, multiplicative factor A was introduced to account for non-ideal experimental losses arising from scattering, surface imperfections, and optical alignment. The resulting model for the transmittance, given by Equations (5), was fitted to the experimental data using a least-squares procedure. The fitted Cauchy parameters were subsequently used to obtain the refractive index spectrum of the NaCl substrate (see **Figure 3(b)**) [20] [21].

$$n(\lambda) = A_n + \frac{B_n}{\lambda^2}$$

$$\delta(\lambda) = \frac{4\pi nd}{\lambda}$$

$$R(n) = \left(\frac{n-1}{n+1}\right)^2 \tag{5}$$

$$F(R) = \frac{4R}{(1-R)^2}$$

$$T = \frac{A}{1 + F\sin^2\left(\frac{\delta}{2}\right)}$$

where R and T denote the reflectance and transmittance of the system, respectively.

3.2. Optical Contrast of Graphene

A strong dependence of graphene optical contrast on substrate type was observed.

For graphene on Si/SiO_2, the optical contrast strongly depended on both the SiO_2 thickness and illumination wavelength due to interference effects between reflected light waves. Figure 4(a) shows the calculated optical contrast for the SiO_2 thickness used in this work (d = 306 nm) as a function of both wavelength and the number of graphene layers. The characteristic wavelengths associated with the red (R), green (G), and blue (B) channels of the image acquisition system are also indicated. Figure 4(b) compares the experimental optical contrast values with the theoretical predictions calculated for different graphene layer numbers using the green channel. From this comparison, it was possible to estimate the number of layers in each sample by identifying regions whose optical contrast matched the expected values for monolayer, bilayer, or multilayer graphene.

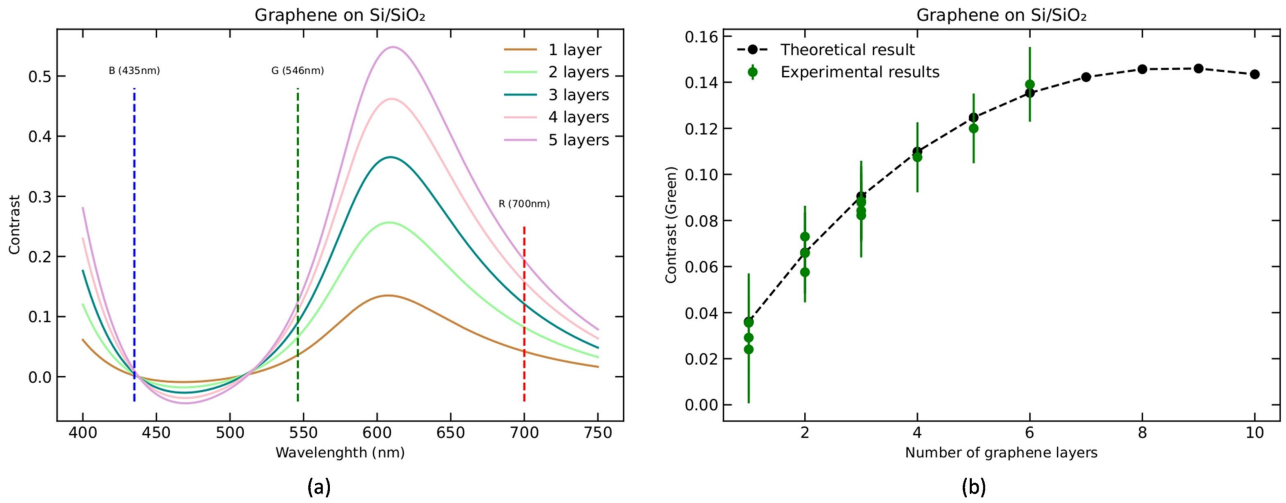

Figure 4. Theoretical and experimental optical contrast results for graphene on Si/SiO_2, obtained using the multilayer interference model as a function of the number of graphene layers and wavelength. (a) Dependence of the optical contrast of graphene deposited on Si/SiO_2 (SiO_2 thickness = 306 nm) as a function of the number of graphene layers and the wavelength of the incident light. (b) Comparison between the theoretical and experimental optical contrast in the green (G) channel as a function of the number of multilayer graphene sheets on a Si/SiO_2 substrate.

In contrast, graphene deposited on NaCl exhibited negative optical contrast, meaning that graphene reflected lighter than the substrate itself. Furthermore, the optical contrast showed weaker wavelength dependence compared to Si/SiO_2 systems (see Figure 5(a)). Contrary to the theoretical predictions, which suggested that the blue channel would provide the highest sensitivity to optical contrast variations, the experimental results reveal a stronger optical contrast in the green channel. This discrepancy can be primarily attributed to the higher sensitivity of the CMOS sensor in the green region of the visible spectrum [22]. Consequently,

the green channel was selected for the experimental determination of the optical contrast.

Figure 5(b) also compares the experimental optical contrast values obtained from the green channel with the theoretical values calculated for different numbers of graphene layers.

As shown in Figure 5(b), the theoretical optical contrast curve for graphene on NaCl is in close agreement with the experimental measurements, with the predicted values remaining within the experimental error bars. The slight deviations between the theoretical and experimental values are consistent with local surface roughness and thickness variations associated with the highly textured NaCl substrate, which are not explicitly considered in the idealized transfer-matrix calculations based on perfectly flat interfaces.

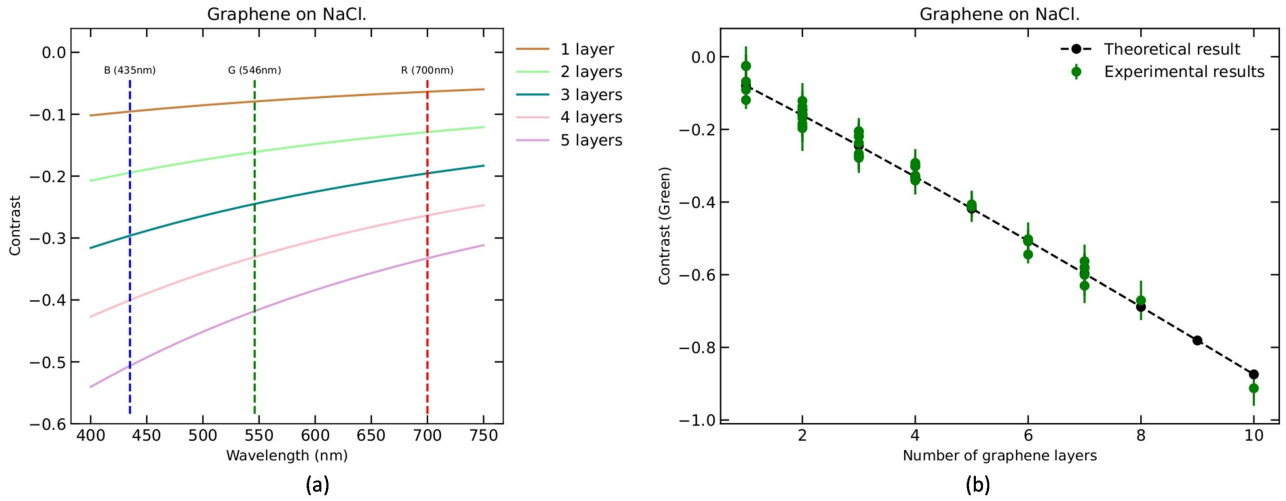

Figure 5. Theoretical and experimental optical contrast results for graphene on NaCl. (a) Dependence of the optical contrast of graphene deposited on NaCl as a function of the number of graphene layers and the wavelength of the incident light. Results obtained from the experimental refractive index determined in this work. (b) Comparison between the theoretical and experimental optical contrast in the green channel (G) as a function of the number of multilayer graphene sheets on a NaCl substrate.

These results demonstrate that NaCl modifies the optical response of graphene differently from conventional dielectric substrates.

3.3. Raman Spectroscopy Analysis

Raman spectroscopy confirmed the presence of multilayer graphene and enabled layer identification through analysis of the 2D band shape. The D band intensity remained low in most samples, indicating relatively high crystalline quality and low defect density.

The 2D peak was analyzed through a deconvolution procedure using Lorentzian fitting functions. A single Lorentzian function was employed for monolayer graphene, whereas four, six, and three Lorentzian components were used for bilayer, trilayer, and four-layer graphene samples, respectively [13] [23] [24].

Figure 6 presents a comparison between the number of graphene layers esti-

mated by optical contrast analysis and that determined from Raman spectroscopy for samples deposited on each substrate (**Figure 6(a)** for Si/SiO_2 and **Figure 6(b)** for NaCl). For the majority of the analyzed samples, both methods yielded consistent results, validating the methodology employed and confirming the reliability of optical contrast measurements as a tool for determining the number of graphene layers.

The Raman spectral shifts were analyzed using the ω_G versus ω_{2D} correlation diagram (see **Figure 7**). In graphene, both the G- and 2D-band frequencies are strongly influenced by charge-carrier doping and mechanical strain, making the interpretation of Raman spectra particularly challenging. Specifically, the G band exhibits a blue shift under both electron and hole doping, whereas the 2D band responds differently depending on the type of induced charge carrier, shifting toward higher frequencies under p-type doping and toward lower frequencies under n-type doping [19] [25].

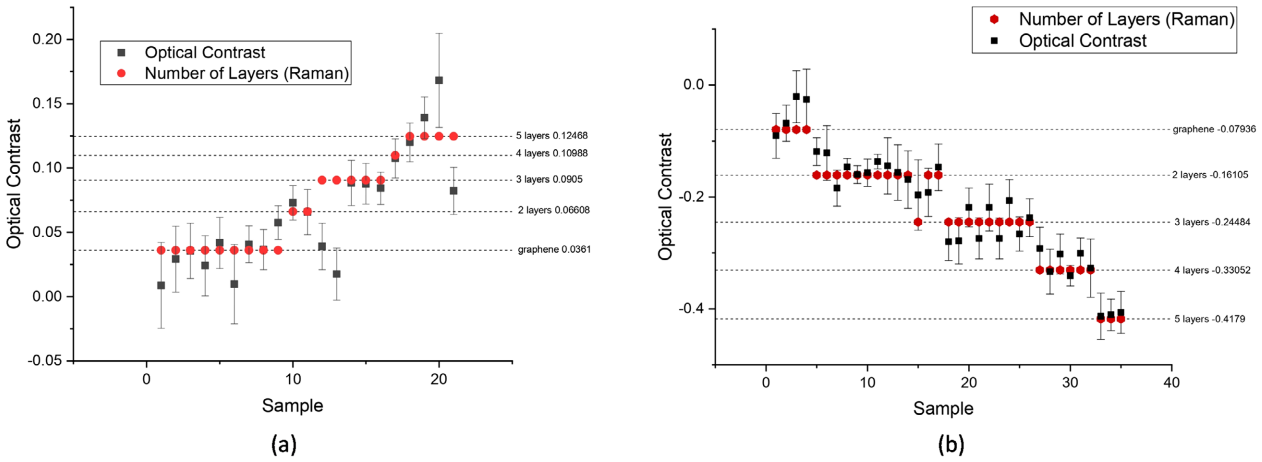

Figure 6. (a) Comparison of the number of graphene layers on a Si/SiO_2 substrate determined by optical contrast and Raman spectroscopy. (b) Comparison of the number of graphene layers on a NaCl substrate determined by optical contrast and Raman spectroscopy.

Mechanical deformation of the graphene lattice also affects the Raman spectrum by modifying the force constants of the carbon-carbon bonds. Tensile strain increases the interatomic distance, resulting in a red shift of both the G and 2D bands. Conversely, compressive strain produces a blue shift. It is worth noting that the 2D mode is considerably more sensitive to strain than the G mode [16]-[18].

To systematically separate the mechanical and electronic contributions of the substrate to the graphene lattice, we employed the Raman vector analysis framework pioneered by Lee *et al.* [19]. This method utilizes the distinct sensitivities of the G and 2D peak positions (ω_G, ω_{2D}) to decouple the effects of hydrostatic/axial strain from charge carrier doping, as the ratio of their shifts ($\Delta\omega_{2D}/\Delta\omega_G$) follows specific trajectories depending on the dominant mechanism [26]. In the $\omega_G - \omega_{2D}$ correlation diagram (**Figure 7**), characteristic vectors corresponding to pure dop-

ing and pure strain effects can be identified. The experimental Raman shifts were therefore decomposed with respect to the reference position of pristine, undoped, and strain-free exfoliated graphene (ω_{2D}^{0} = 2676.9 and ω_{G}^{0} = 1581.6), adopted from the standard literature baseline for 532 nm (2.33 eV) laser excitation [19] (Figure 7). These coordinates represent the ideal charge-neutrality and zero-strain point in the ω_{2D} vs. ω_{G} correlation space. By projecting each experimental data point ($\boldsymbol{P}$) onto the doping and strain axes, the individual contributions of these two effects were quantitatively determined as follows:

$$\boldsymbol{P} = a\hat{e}_T + b\hat{e}_H \tag{6}$$

where a and b are scalar coefficients, while $\hat{e}_T$ and $\hat{e}_H$ denote the unit vectors corresponding to the characteristic directions of tensile strain ($\Delta\omega_{2D}/\Delta\omega_{G}$ = 2.2 ± 0.2) and hole doping ($\Delta\omega_{2D}/\Delta\omega_{G}$ = 0.70 ± 0.05), respectively [19].

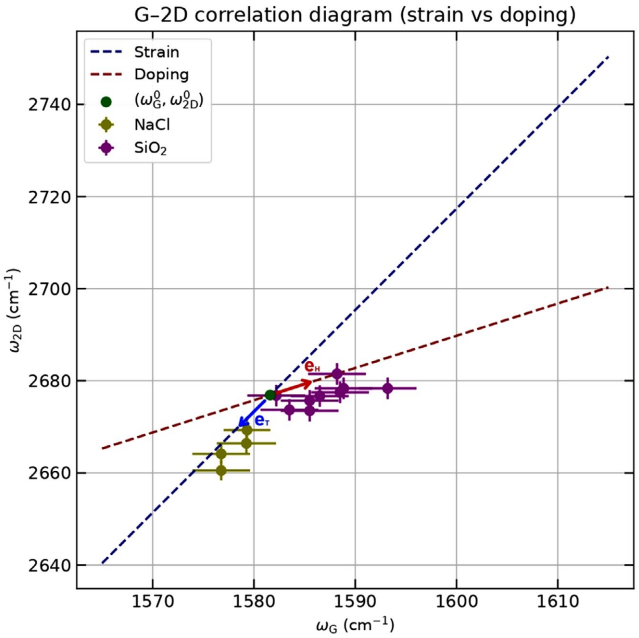

Figure 7. ω_{2D} versus ω_{G} correlation diagram for graphene deposited on SiO_2 and NaCl substrates, illustrating the vector decomposition into mechanical strain and doping axes.

This procedure made it possible to extract the net G-band shift arising exclusively from doping ($\Delta\omega_{G}^{doping}$) by removing the contributions associated with mechanical strain.

Analysis of the ω_{G} − ω_{2D} correlation diagram for graphene deposited on SiO_2 reveals a significant variation in the G-band position, on the order of ~11 cm^{-1}, while the 2D band remains relatively stable. This behavior indicates that doping is the dominant effect in this system, since the G band is highly sensitive to carrier concentration, whereas the 2D band exhibits a weaker dependence in this regime. Furthermore, the direction of the shifts in the ω_{G} − ω_{2D} diagram, together with the trends observed in Figure 8(a), indicates that the samples are predominantly p-

doped, implying that the Fermi level is shifted below the Dirac point.

In contrast, graphene deposited on NaCl exhibits a markedly different behavior. In this case, a general downshift of the G band is observed, accompanied by a substantial variation in the 2D-band position of approximately ~13 cm^{-1}. This pattern is characteristic of a regime in which mechanical strain, rather than doping, is the dominant effect. In particular, the simultaneous downshift of both the G and 2D bands (see **Figure 8(b)** and **Figure 8(c)**) is indicative of tensile strain in the graphene lattice. This behavior is likely associated with the highly textured nature of the NaCl substrates. The dispersion of the experimental data further suggests that this strain is not uniform across the samples but exhibits significant local variations. Such behavior may be associated with weaker graphene-substrate adhesion, surface roughness of the NaCl substrate, or residual stresses introduced during the transfer process.

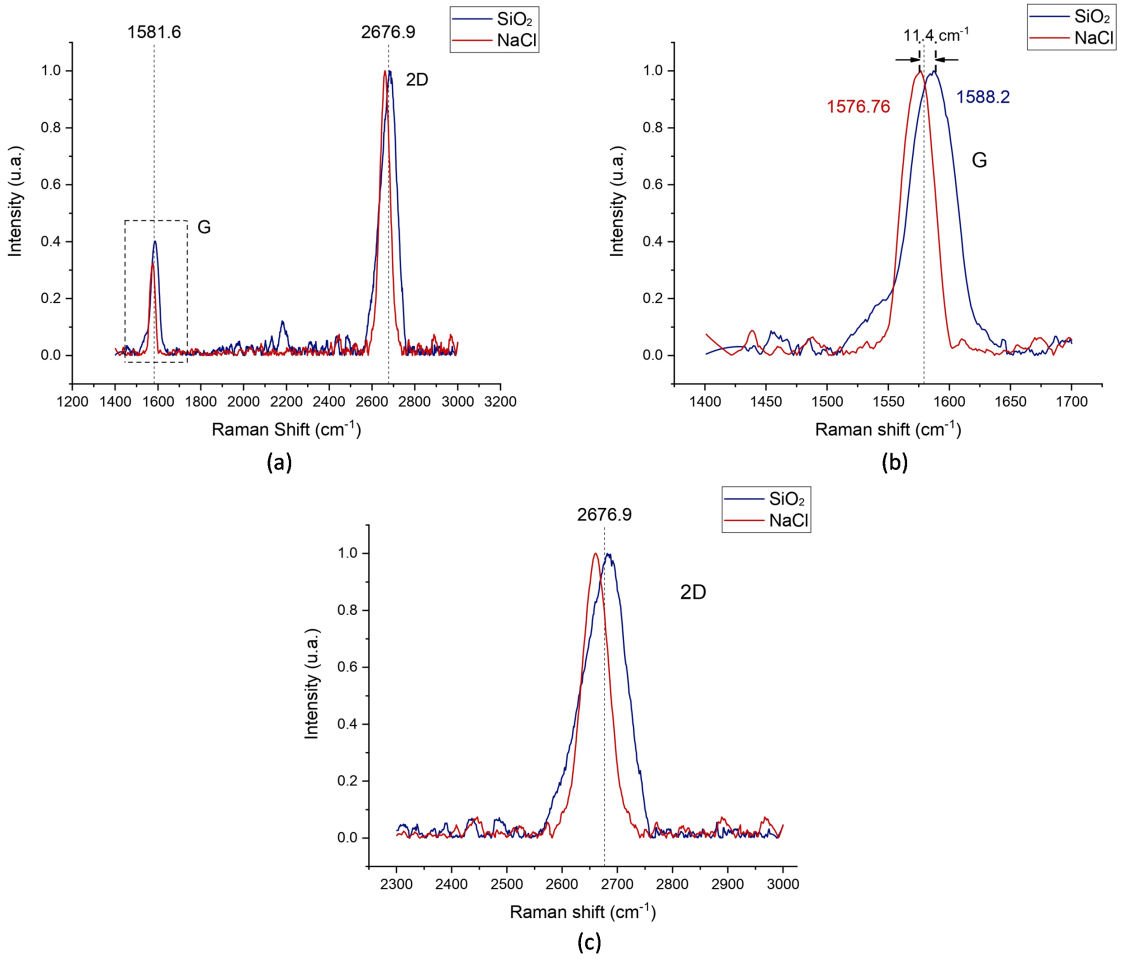

Figure 8. (a) Representative Raman spectra of graphene deposited on Si/SiO_2 (blue) and NaCl (red) substrates. The characteristic G and 2D bands are indicated, along with the reference positions for charge-neutral graphene (dashed lines). (b) Expanded and normalized Raman spectra in the 1400 cm^{-1} - 1700 cm^{-1} spectral range, showing the shift of the G band for graphene deposited on different substrates. (c) Expanded and normalized Raman spectra in the 2300 cm^{-1} - 3000 cm^{-1} spectral range, highlighting the differences in the 2D-band position for graphene deposited on Si/SiO_2 and NaCl substrates.

To assess whether substrate morphology could contribute to the Raman shifts observed in graphene on NaCl, the surface topography of the NaCl substrate used for graphene deposition was examined by Atomic Force Microscopy (AFM), as shown in Figure 9. The AFM image reveals a crystalline surface with terraces and nanoscale corrugations, with a root-mean-square roughness of $R_q \approx 3.1$ nm over a 2×2 μm^2 area.

Compared with the typically smoother surface of thermally grown SiO_2, the NaCl substrate exhibits a more pronounced nanoscale texture that may locally modify the graphene conformation and induce non-uniform strain fields during exfoliation and transfer. However, the AFM results primarily demonstrate that surface roughness is present and has been quantified, while the Raman shifts observed in this work are interpreted as arising from a combination of substrate-induced strain and electronic interactions rather than from surface roughness alone.

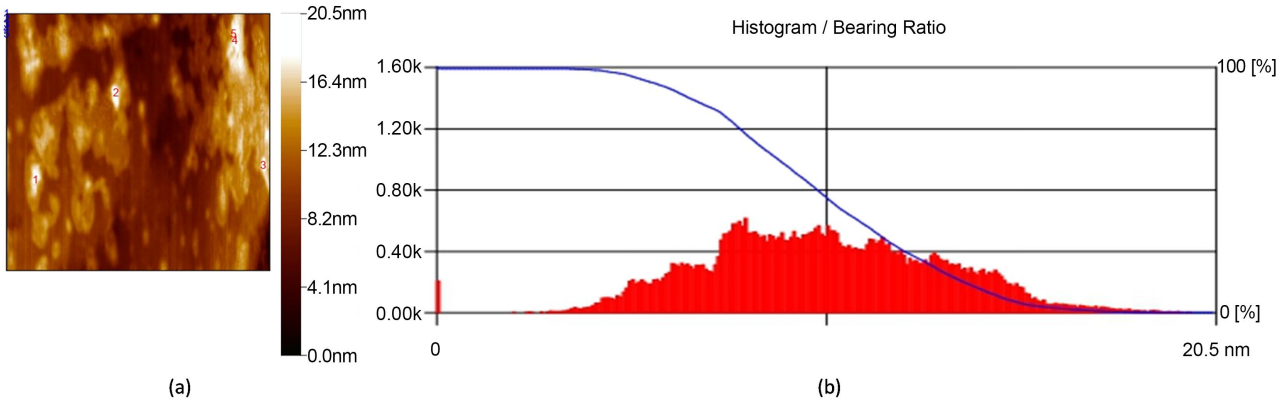

Figure 9. (a) AFM topography image of the NaCl substrate used for graphene deposition. (b) Corresponding height distribution extracted from the AFM data. The surface exhibits an RMS roughness of $R_q = 3.1$ nm over a 2×2 μm^2 area.

Substrate-induced nanoscale curvatures and step edges are known to act as local pinning centers, generating micro-strain variations across the graphene flake [27]. According to molecular models of graphene on non-flat substrates, topography-induced conformal changes lead to non-uniform tensile or compressive strain, which heavily modulates the Raman phonon frequencies and broadens the linewidths [28]. This observation may help explain why mechanical deformation appears to play a more prominent role in graphene on textured NaCl substrates compared with flatter, amorphous SiO_2 surfaces.

These results indicate that, while SiO_2 primarily influences the electronic properties of graphene through substrate-induced doping, NaCl predominantly affects its mechanical state by introducing local strain.

From the doping component obtained through the vector decomposition analysis, it is possible to estimate the shift of the Fermi level relative to the Dirac point and, consequently, determine the carrier concentration in each sample. The Fermi energy, E_F, of graphene was estimated from the shift of the G peak exclusively

associated with doping ($\Delta\omega_{\mathrm{G}}^{\mathrm{doping}}$), according to Equation (7):

$$\left|E_F\left(\mathrm{eV}\right)\right| \approx \frac{\Delta\omega_{\mathrm{G}}^{\mathrm{doping}}}{42} \tag{7}$$

where $\Delta\omega_{\mathrm{G}}^{\mathrm{doping}}$ corresponds to the G-band shift solely attributable to charge-carrier doping.

This expression stems from a well-established linear approximation rooted in the electron-phonon coupling (EPC) theory of graphene. Physically, when charge carriers are introduced, the Fermi level shifts away from the Dirac point. For moderate doping regimes where $|E_F|$ exceeds half of the optical phonon energy ($|E_F| > \hbar\omega_{ph}/2 \approx 0.1\,\mathrm{eV}$), interband electron-phonon transitions are effectively blocked due to the Pauli exclusion principle. This phenomenon modifies the phonon self-energy, leading to a dynamic renormalization and hardening (blueshift) of the Γ-point E_{2g} optical modes (G band). Although the rigorous perturbation theory yields a complex logarithmic dependence, the relationship can be linearized with high accuracy within the 0.1 - 0.4 eV range. The calibration factor of $\approx 42\,\mathrm{cm}^{-1}/\mathrm{eV}$ utilized here represents the widely accepted empirical sensitivity of the G-band position to the Fermi energy in supported graphene architectures, as validated by electrostatically gated calibrations [16]-[18] [29] [30].

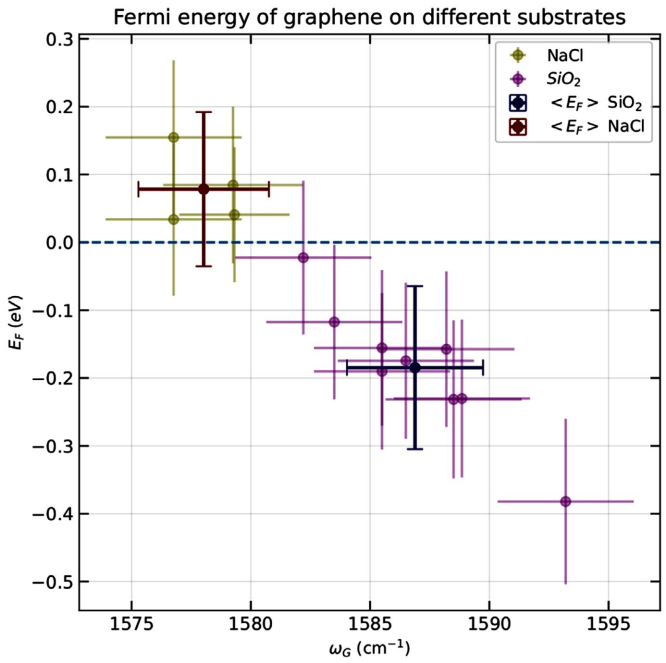

Figure 10. Average Fermi energy of graphene deposited on SiO_2 and NaCl substrates, including the corresponding error bars.

Figure 10 presents the average Fermi energy values obtained for graphene supported on SiO_2 and NaCl substrates, including the corresponding uncertainties represented by the error bars. The values obtained were:

$$E_F\left(\mathrm{SiO}_2\right) \approx -0.176 \pm 0.119\ \mathrm{eV}$$

$$E_F\left(\mathrm{NaCl}\right) \approx 0.078 \pm 0.114 \text{ eV}$$

Graphene deposited on SiO_2 exhibits Fermi energy values that, together with the upshift of the 2D band observed in **Figure 8(c)**, are consistent with p-type doping. In contrast, the graphene samples deposited on NaCl show Fermi energies ranging from approximately 12 meV to 116 meV, indicating a moderate doping level. Combined with the downshift of the 2D band toward lower frequencies observed in **Figure 8(c)**, these results are indicative of n-type doping.

This behavior offers an intriguing contrast to other crystalline ionic environments reported in the literature. For example, graphene supported on mica substrates typically experiences strong p-type doping, which is generally attributed to water-gated charge transfer from ambient moisture trapped at the hydrophilic, potassium-rich cleaved surface [10]. In our case, the highly textured NaCl lattice likely promotes a different electrostatic gating mechanism or chemical interaction at the interface, suppressing the conventional ambient p-doping and favoring electron accumulation. This highlights the capacity of alkali halide substrates to tune the carrier type of 2D materials via intrinsic electrostatic substrate effects.

The analysis revealed:

- Graphene on SiO_2 exhibited predominant p-type doping.
- Graphene on NaCl showed a tendency toward n-type doping.
- Strain effects contributed significantly to the Raman shifts in NaCl-supported samples.

It should be noted, however, that factors other than the substrate itself may also contribute to the observed Raman shifts. In particular, adsorbed water or oxygen molecules, residual contamination originating from the mechanical exfoliation process, and local laser-heating effects may influence the measured doping levels. Therefore, although the observed trends are consistent with a substrate-induced contribution associated with the ionic nature of NaCl, the present study cannot completely disentangle these effects. Future investigations under controlled environmental conditions will be necessary to isolate the specific contribution of the substrate.

The carrier concentration n was subsequently estimated from the calculated Fermi energy according to Equation (8):

$$n = \frac{E_F^2}{\pi\left(\hbar v_F\right)^2} \tag{8}$$

where $v_F \approx 1.1\times10^6$ m/s denotes the Fermi velocity of graphene [31].

The average carrier concentrations were estimated to be 2.6×10^{12} cm^{-2} for graphene on SiO_2 and 0.5×10^{12} cm^{-2} for graphene on NaCl, values that are typical of moderately doped supported graphene systems.

3.4. Substrate-Induced Effects

The observed differences between graphene on SiO_2 and NaCl demonstrate the critical role played by substrate-induced electrostatic interactions.

Unlike SiO_2, NaCl provides a periodic ionic surface potential that may influence graphene charge distribution and Fermi level position. To understand the physical origin of the observed tendency toward n-type doping on NaCl substrates, the electrostatic environment at the graphene/substrate interface must be considered. In an ideal atomically flat NaCl (100) surface, the electrostatic potentials generated by the alternating Na^+ and Cl^- ions are largely compensated by crystal symmetry. However, the highly textured morphology of our NaCl substrates introduces a large density of surface corrugations, terraces, and step edges, where this local symmetry is partially broken.

These morphological features can generate localized electrostatic fields and surface dipoles that modify the electronic environment experienced by the graphene layer. When graphene conforms to such a textured ionic surface, these local electrostatic potentials may induce charge redistribution within the graphene sheet and shift its Fermi level relative to the Dirac point. This effect provides a plausible explanation for the systematic tendency toward n-type doping observed in our Raman analysis.

A similar interpretation has been proposed for graphene interacting with charged or ionic substrates, where local electrostatic fields and interfacial dipoles influence the carrier concentration without requiring direct chemical bonding [10] [32]. In the present case, the combination of the ionic nature of NaCl and its pronounced surface texturing may therefore contribute to the observed electron-doping tendency [28]. Nevertheless, contributions from adsorbates [33], transfer-induced residues [34], or other substrate-related effects cannot be completely excluded and may also play a role in the measured carrier concentrations.

4. Conclusions

Multilayer graphene was successfully synthesized through mechanical exfoliation and deposited onto NaCl substrates. XRD and UV-Vis characterization confirmed the high crystalline quality and optical transparency of the NaCl substrates.

Optical contrast measurements revealed substantial differences between graphene on Si/SiO_2 and graphene on NaCl. In particular, graphene on NaCl exhibited negative optical contrast and weaker wavelength dependence.

Raman spectroscopy demonstrated that substrate induced effects significantly modify graphene properties. Graphene supported on SiO_2 presented predominant p-type doping, whereas graphene on NaCl exhibited a tendency toward n-type doping with important strain contributions.

Overall, these findings underscore the importance of substrate selection in graphene-based devices and reveal NaCl single crystals as a promising platform for studying substrate-induced electrostatic effects in two-dimensional materials. In addition, the successful deposition and characterization of mechanically exfoliated graphene on NaCl validate the feasibility of this approach and establish a methodology that, to the best of our knowledge, has not been systematically reported previously.

Acknowledgements

The authors gratefully acknowledge M.Sc. Salvador López Morales for providing access to the Raman spectrometer, an essential resource for obtaining the results presented in this work. They also thank M.Sc. Adriana Tejeda Cruz for her assistance with the X-ray diffraction (XRD) measurements of the NaCl substrates used in this study. The authors further acknowledge Physicist Carlos Flores Morales for acquiring and providing the Atomic Force Microscopy (AFM) images that enabled the surface morphology analysis of the NaCl substrates. Finally, the authors express their sincere gratitude to Dr. D. E. Martínez Lara for his guidance and training in the operation of the Raman spectrometer, which was instrumental to the experimental development of this project.

Author Contributions

Conceptualization, D. Mendoza Lopez; methodology, D. Mendoza Lopez; investigation, R. Antolin-Jimenez; experiments and data collection, R. Antolin-Jimenez; writing—original draft preparation, R. Antolin-Jimenez; writing—review and editing, R. Antolin-Jimenez and D. Mendoza Lopez; supervision, D. Mendoza Lopez. Both authors have read and agreed to the published version of the manuscript.

Conflicts of Interest

The authors declare no conflicts of interest regarding the publication of this paper.

References

[1] Novoselov, K.S., Geim, A.K., Morozov, S.V., Jiang, D., Zhang, Y., Dubonos, S.V., *et al.* (2004) Electric Field Effect in Atomically Thin Carbon Films. *Science*, **306**, 666-669. https://doi.org/10.1126/science.1102896

[2] Lee, C., Wei, X., Kysar, J.W. and Hone, J. (2008) Measurement of the Elastic Properties and Intrinsic Strength of Monolayer Graphene. *Science*, **321**, 385-388. https://doi.org/10.1126/science.1157996

[3] Griffith, A.A. (1921) VI. The Phenomena of Rupture and Flow in Solids. *Philosophical Transactions of the Royal Society of London. Series A, Containing Papers of a Mathematical or Physical Character*, **221**, 163-198. https://doi.org/10.1098/rsta.1921.0006

[4] Pantano, M.F., Iacob, E., Picciotto, A., Margesin, B., Centeno, A., Zurutuza, A., *et al.* (2019) Investigation of Charges-Driven Interactions between Graphene and Different SiO_2 Surfaces. *Carbon*, **148**, 336-343. https://doi.org/10.1016/j.carbon.2019.03.071

[5] Nowak, D., Clapa, M., Kula, P., Sochacki, M., Stonio, B., Galazka, M., *et al.* (2019) Influence of the Interactions at the Graphene-Substrate Boundary on Graphene Sensitivity to UV Irradiation. *Materials*, **12**, Article No. 3949. https://doi.org/10.3390/ma12233949

[6] Kong, W., Li, H., Qiao, K., Kim, Y., Lee, K., Nie, Y., *et al.* (2018) Polarity Governs Atomic Interaction through Two-Dimensional Materials. *Nature Materials*, **17**, 999-1004. https://doi.org/10.1038/s41563-018-0176-4

[7] Mendoza, D. (2000) The Cooper Pair Problem in an External Periodic Potential. *Re-*

vista Mexicana de Física, **46**, 304-308.

[8] Bautista-Flores, C., Sato-Berrú, R.Y. and Mendoza, D. (2018) Raman Spectroscopy of CVD Graphene during Transfer Process from Copper to SiO_2/Si Substrates. *Materials Research Express*, **6**, Article ID: 015601. https://doi.org/10.1088/2053-1591/aae32f

[9] Mishra, N., Rossi, A., Martini, L., Chianese, F., Magnozzi, M., Canepa, M., *et al.* (2026) Spontaneous Intercalation of Graphene on Sapphire. *Small Methods*, **10**, e02396. https://doi.org/10.1002/smtd.202502396

[10] Shim, J., Lui, C.H., Ko, T.Y., Yu, Y., Kim, P., Heinz, T.F., *et al.* (2012) Water-Gated Charge Doping of Graphene Induced by Mica Substrates. *Nano Letters*, **12**, 648-654. https://doi.org/10.1021/nl2034317

[11] Bautista-Flores, C. and Mendoza, D. (2014) Modulación de las propiedades electrónicas de multicapas de grafeno por un material iónico. *Proceedings of the VII Congreso Internacional de Ingeniería Física*, Mexico City, 24-28 November 2014, 1.

[12] Bautista Flores, C. Grafeno Graphene, YouTube Video. https://www.youtube.com/watch?v=h9KvTgidDzg

[13] Bautista Flores, C., Sato Berrú, R.Y. and Mendoza López, D. (2015) Observación de capas de grafeno mediante contraste óptico y dispersión Raman. *Mundo Nano. Revista Interdisciplinaria en Nanociencias y Nanotecnología*, **6**, 29-39. https://doi.org/10.22201/ceiich.24485691e.2013.11.50002

[14] Lee, H., Lee, K., Ryu, S., Yi, Y., Jeon, J., Kim, S., *et al.* (2022) Nondestructive Thickness Determination of Polymers Based on Optical Contrast of Graphene. *Applied Nanoscience*, **13**, 4427-4435. https://doi.org/10.1007/s13204-022-02710-4

[15] Fowles, G.R. (1989) Introduction to Modern Optics. Courier Corporation.

[16] Piscanec, S., Lazzeri, M., Mauri, F. and Ferrari, A.C. (2007) Optical Phonons of Graphene and Nanotubes. *The European Physical Journal Special Topics*, **148**, 159-170. https://doi.org/10.1140/epjst/e2007-00236-2

[17] Pisana, S., Lazzeri, M., Casiraghi, C., Novoselov, K.S., Geim, A.K., Ferrari, A.C., *et al.* (2007) Breakdown of the Adiabatic Born-Oppenheimer Approximation in Graphene. *Nature Materials*, **6**, 198-201. https://doi.org/10.1038/nmat1846

[18] Jnawali, G., Rao, Y., Beck, J.H., Petrone, N., Kymissis, I., Hone, J., *et al.* (2015) Observation of Ground- and Excited-State Charge Transfer at the C_{60}/Graphene Interface. *ACS Nano*, **9**, 7175-7185. https://doi.org/10.1021/acsnano.5b01896

[19] Lee, J.E., Ahn, G., Shim, J., Lee, Y.S. and Ryu, S. (2012) Optical Separation of Mechanical Strain from Charge Doping in Graphene. *Nature Communications*, **3**, Article No. 1024. https://doi.org/10.1038/ncomms2022

[20] Jenkins, F.A., White, H.E. and Brukhard, D.G. (1958) Fundamentals of Optics. *American Journal of Physics*, **26**, Article No. 272. https://doi.org/10.1119/1.1996127

[21] Born, M. and Wolf, E. (1970) Principles of Optics. Pergamon Press.

[22] FRAMOS, FSM-IMX335 Datasheet, FRAMOS GmbH (2019), Sony IMX335 Sensor Module. https://www.mouser.com/datasheet/2/1051/FSM-IMX335_Datasheet_v1-0f_Brief7yNk6lBv2AQtC-1815700.pdf

[23] Malard, L.M., Pimenta, M.A., Dresselhaus, G. and Dresselhaus, M.S. (2009) Raman Spectroscopy in Graphene. *Physics Reports*, **473**, 51-87. https://doi.org/10.1016/j.physrep.2009.02.003

[24] Ferrari, A.C., Meyer, J.C., Scardaci, V., Casiraghi, C., Lazzeri, M., Mauri, F., *et al.* (2006) Raman Spectrum of Graphene and Graphene Layers. *Physical Review Letters*,

97, Article ID: 187401. https://doi.org/10.1103/physrevlett.97.187401

[25] Das, A., Pisana, S., Chakraborty, B., Piscanec, S., Saha, S.K., Waghmare, U.V., *et al*. (2008) Monitoring Dopants by Raman Scattering in an Electrochemically Top-Gated Graphene Transistor. *Nature Nanotechnology*, **3**, 210-215. https://doi.org/10.1038/nnano.2008.67

[26] Ott, A.K. and Ferrari, A.C. (2024) Raman Spectroscopy of Graphene and Related Materials. In: *Encyclopedia of Condensed Matter Physics*, 2nd Edition, Elsevier, 233-247. https://doi.org/10.1016/b978-0-323-90800-9.00252-3

[27] Neumann, C., Reichardt, S., Venezuela, P., Drögeler, M., Banszerus, L., Schmitz, M., *et al*. (2015) Raman Spectroscopy as Probe of Nanometre-Scale Strain Variations in Graphene. *Nature Communications*, **6**, Article No. 8429. https://doi.org/10.1038/ncomms9429

[28] Zhang, Y., Heiranian, M., Janicek, B., Budrikis, Z., Zapperi, S., Huang, P.Y., *et al*. (2018) Strain Modulation of Graphene by Nanoscale Substrate Curvatures: A Molecular View. *Nano Letters*, **18**, 2098-2104. https://doi.org/10.1021/acs.nanolett.8b00273

[29] Lazzeri, M. and Mauri, F. (2006) Nonadiabatic Kohn Anomaly in a Doped Graphene Monolayer. *Physical Review Letters*, **97**, Article ID: 266407. https://doi.org/10.1103/physrevlett.97.266407

[30] Bautista-Flores, C., Sato-Berrú, R.Y. and Mendoza, D. (2015) Doping Graphene by Chemical Treatments Using Acid and Basic Substances. *Journal of Materials Science and Chemical Engineering*, **3**, 17-21. https://doi.org/10.4236/msce.2015.310003

[31] Chen, C., Park, C., Boudouris, B.W., Horng, J., Geng, B., Girit, C., *et al*. (2011) Controlling Inelastic Light Scattering Quantum Pathways in Graphene. *Nature*, **471**, 617-620. https://doi.org/10.1038/nature09866

[32] Lafkioti, M., Krauss, B., Lohmann, T., Zschieschang, U., Klauk, H., Klitzing, K.V., *et al*. (2010) Graphene on a Hydrophobic Substrate: Doping Reduction and Hysteresis Suppression under Ambient Conditions. *Nano Letters*, **10**, 1149-1153. https://doi.org/10.1021/nl903162a

[33] Ryu, S., Liu, L., Berciaud, S., Yu, Y., Liu, H., Kim, P., *et al*. (2010) Atmospheric Oxygen Binding and Hole Doping in Deformed Graphene on a SiO_2 Substrate. *Nano Letters*, **10**, 4944-4951. https://doi.org/10.1021/nl1029607

[34] Pirkle, A., Chan, J., Venugopal, A., Hinojos, D., Magnuson, C.W., McDonnell, S., *et al*. (2011) The Effect of Chemical Residues on the Physical and Electrical Properties of Chemical Vapor Deposited Graphene Transferred to SiO_2. *Applied Physics Letters*, **99**, Article ID: 122108. https://doi.org/10.1063/1.3643444